

Challenges of interpreting dielectric dilatometry for the study of pressure densification

Alejandro Sanz,* Jeppe C. Dyre, and Kristine Niss
*Glass and Time, IMFUFA, Department of Science and Environment,
Roskilde University, Postbox 260, DK-4000 Roskilde, Denmark*
(Dated: February 28, 2019)

We report an experimental study documenting the challenge of employing dielectric dilatometry for the study of pressure densification in glass-forming materials. An influence of the dielectric cell geometry on the resulting capacitance of 5-poly-phenyl-ether upon vitrification under different thermobaric pathways is documented. The capacitive response is studied for two different multilayer capacitors: one with, in principle, fixed plate distance and one with Kapton® spacers allowing for contraction/expansion. A combination of changes in the dielectric permittivity of the material and modifications of the capacitor geometry determines the final capacitance. We conclude that, in order to convert the measured capacitance to material density, it is of paramount importance to understand the geometry. The data presented do not make it possible to conclude on whether or not simple glass formers such as 5-poly-phenyl-ether can be pressure densified, but our work highlights the challenge of utilizing dielectric spectroscopy to tackle this problem effectively.

PACS numbers: 64.70.kj, 64.70.pm, 62.50.-p, 77.22.-d.

I. INTRODUCTION

Density as a function of temperature and pressure is among the most fundamental thermodynamic and structural parameters of a glass-forming liquid, and the abrupt change in the temperature and pressure derivatives of density, the thermal expansion coefficient and the compressibility, are a principal signature of the glass transition [1]. Low-molecular-weight glass-forming liquids are often used in fundamental research on the glass transition [2–6]. However, measuring the density in the glass transition region is difficult for these liquids due to their low glass transition temperatures. Most techniques for measuring density rely on a confining liquid and are limited by the temperature-pressure range where it is in its liquid state, e.g. mercury which has a melting point of 234.3 K at atmospheric pressure. This challenge has the consequence that a fundamental result like density scaling to a large extent is based on extrapolated density data when it comes to molecular liquids [7–9].

An alternative method for measuring density is dielectric dilatometry [10, 11]. This technique makes use of the fact that the dielectric constant of a material depends on the number density of molecules (and number density is proportional to mass density, as long as no chemical reactions take place). The advantage of dielectric dilatometry is that it can be measured with very high precision and that it can be applied at low temperatures. The method has been used in several studies of scanning dilatometry of polymer films where it has the additional advantage of getting more precise with a thinner film [10, 12–14]. It has also been used for measuring the dynamic linear expansion coefficient where the high precision gained by this method is crucial for obtaining the resolution needed to measure in the linear range [10, 11, 15]. Recently, the

method has been employed to study pressure densification of a molecular glass [16]. While dielectric dilatometry has potential to be used more in the field, it also has some limitations. In this paper we investigate these limitations with a focus on the challenges connected to study pressure densification.

Pressure densification refers to a situation where a glass formed by cooling at elevated pressures and subsequently decompressed in the glassy state, has a higher density than a glass of the same material formed by cooling at low pressures. It is a physical phenomenon widely known in inorganic glasses, such as silica [17–19], that can be used for tuning its optical properties [20]. Roland and colleagues recently proposed a new approach for examining pressure densification from a more fundamental point of view. They suggested examining the problem under the framework of the isomorph theory [16, 21, 22], which predicts the existence of isomorphs in the so-called R-simple systems [23]. Pressure densification is also a long-standing topic in the physics of polymeric materials that has been investigated both experimentally and theoretically, for instance in polymethylmethacrylate (PMMA) and in other amorphous polymers [22, 24, 25]. Pressure densification has also been studied in polymeric systems by computer simulations [21]. The fact that PMMA can be pressure densified is somewhat surprising since this polymer conforms with isochronal superposition and density scaling [26], and therefore it is likely to behave as a "Roskilde-simple system" (R-simple) according to the isomorph theory [23, 27].

The increase in density of glasses prepared under high pressure was found to vary from 1-2 % in molecular glasses and polymers to more than 15 % in inorganic materials [19, 24, 28]. Casalini and Roland proposed a metric for the degree of densification in terms of the relative changes in specific volume for vitrification at high and low pressures. This so-called pressure densification ratio, δ , was estimated to be around 25 % for densification pressures between 300 and 570 MPa in the molecular glass-

* asanz@ruc.dk

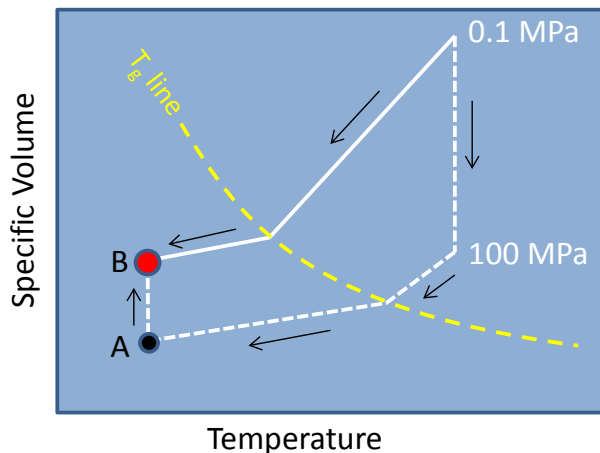


FIG. 1. Schematic phase diagram showing the dependence of specific volume with temperature at 0.1 and 100 MPa upon cooling through the glass transition. Solid and dashed white lines describe the thermodynamic routes for reaching the state point B explored in this work. The dashed yellow line corresponds to the T_g line.

former tetramethyl-tetraphenyl-siloxane (DC704) [16].

The recent interest in pressure densification from a more fundamental point of view is sparked by the prediction that R-simple liquids cannot be pressure densified [21, 29]. Isomorph theory predicts that all glasses formed along the same glass-transition isochrone (for example formed with the same cooling rate at different pressures) will have the same microscopic structure, except for the average distance between the molecules which will scale with the cubic root of the inverse density. If the pressure is released on a glass formed at high pressure, then the average molecular distance will increase, and the glass will attain the same density as the glass formed at lower pressures. This has been supported by simulations but some experiments contradict this prediction [16, 22, 28].

In this study, we have investigated experimentally two temperature-pressure protocols, using two different dielectric cells in order to highlight the role of macroscopic geometry in these experiments. A schematic description of the phase diagram explored in this work is illustrated in Fig. 1.

In the following section we present the fundamental principle of dielectric dilatometry. In section III we present the experimental method. Section IV presents the results which are analyzed and discussed in section V.

II. BACKGROUND: DIELECTRIC DILATOMETRY

The fundamental assumption that needs to be fulfilled in order to use dielectric dilatometry is that the high-frequency dielectric permittivity, ϵ_∞ , only depends

on density in the part of pressure-temperature diagram where it is measured. On a quantitative level, the high-frequency dielectric permittivity is connected to molecular properties using the Clausius-Mossotti (CM) relation [30]:

$$\frac{\epsilon_\infty - 1}{\epsilon_\infty + 2} = \frac{n}{3\epsilon_0}\alpha_0, \quad (1)$$

where α_0 is the polarizability of a single molecule, n is the number density of molecules and ϵ_0 is the vacuum permittivity. It is seen from this expression that α_0 needs to be temperature and pressure independent in order for the method to be viable for determining n . In contrast, the polarization due to rotation of permanent dipoles is highly pressure and temperature dependent in glass-forming liquids. In fact, dielectric spectroscopy is among the most commonly applied techniques to investigate dynamics of glass-formers [6, 31]. However, the rotational contribution is frozen out as the glass transition is approached, and if measurements are performed at high frequencies close to the glass transition, the rotational contribution can in many cases be assumed to be negligible. Besides rotation of permanent dipoles, the other contribution to α_0 is the atomic polarization due to deformation of the electron cloud. The atomic polarization takes place instantaneously and it can be assumed to be constant as long as temperatures are much lower than the electronic binding energies. Given the local character of the induced atomic polarization and the modest pressures used in the present study, atomic polarization can be considered pressure-independent, as well.

The CM-relation is derived as a mean field approximation, and is not expected to be exact. Deviations from CM may influence the absolute values found from the method, but will not affect temperature, pressure or time dependence found of the thermal expansion coefficient or the bulk modulus (see Ref. [11] for details).

Given the connection between density and dielectric constant, the next step is to connect the measured capacitance with the dielectric constant. In the simple case with a capacitor completely filled with sample liquid one has

$$C_m = \epsilon_\infty C_g, \quad (2)$$

where C_g is the empty capacitance which is determined by the geometry of the capacitor. For a parallel plate geometry it is given by $C_g = \epsilon_0 A/l$, with l the distance between the plates and A the area.

The measured change in capacitance, following an applied temperature or pressure variation, is a combined effect of the change in dielectric constant and the change in the geometric capacitance

$$dC_m = \epsilon_\infty dC_g + C_g d\epsilon_\infty. \quad (3)$$

The use of dielectric dilatometry consequently relies on assumptions regarding how the geometrical capacitance responds to pressure and temperature changes. What

III. EXPERIMENTAL DETAILS AND MEASURING PRINCIPLE

To investigate the role of capacitor geometry and boundary conditions on pressure densification results, we have studied the same sample with different protocols using two different capacitors. The sample studied is the van der Waals liquid 5-poly-phenyl-ether (5PPE). The sample, with chemical structure shown in Fig. 2(a), was purchased from Santolubes and used as received. Due to its relatively high glass transition temperature (T_g) at atmospheric pressure, 245 K, 5PPE suits the technical specifications of our high-pressure dielectric setup. Furthermore, 5PPE fulfils several prerequisites to be considered an R-simple liquid [9, 32–34], just like tetramethyl-tetraphenyl-siloxane studied in Ref. [16]. In 5PPE we thus expect the existence of isomorphs, that is, lines in the phase diagram along which several structural, dynamic and thermodynamic properties are invariant [9, 23, 32–34]. Isomorphs are also isochrones, which are curves in the phase diagram with constant relaxation time.

Two different multilayer capacitors were used in the study; an air capacitor and a home-built capacitor with Kapton® spacers. Figure 2(c) shows a picture of the air capacitor. It is similar to that used in Ref. [16] and has no spacer material, because the electrode plates are kept apart by the metallic scaffold. The distance between the electrode plates is in the order of half a millimeter and the empty capacitance is 85 pF when measured at ambient conditions. Figure 2(d) shows the home-built multilayer capacitor. The separation between the metallic electrodes is maintained by four spacers made of Kapton® (50 μm thick). The spacers determine the distance when the capacitor is empty or filled with a low viscosity liquid, while the sample itself will determine the distance between the plates for viscosities high enough that the sample cannot flow [11]. Twelve plates are stacked on top of each other forming eleven capacitors in parallel giving a total empty capacitance at ambient conditions of approximately 560 pF.

In both cases, once the dielectric capacitor is filled with the liquid under study at room temperature, it is immersed in a rubber container full of the same sample liquid. This reservoir makes it possible for extra liquid to flow into the capacitor as the liquid contracts upon cooling, a flow that, notably, is only possible at low-viscosity conditions. Successive rubber and teflon layers shield the sample from the pressure-transmitting medium. This configuration is illustrated in the schematic drawing of Fig. 2(b). Detailed information about the dielectric hardware and high-pressure equipment can be found elsewhere [35, 36].

We explored the phase diagram of Fig. 1 by controlling pressure and temperature along the two different pathways. Figure 3 shows the real part of the capacitance for 5PPE at atmospheric pressure at two different temperatures, 275 and 240 K, where the signal is dominated

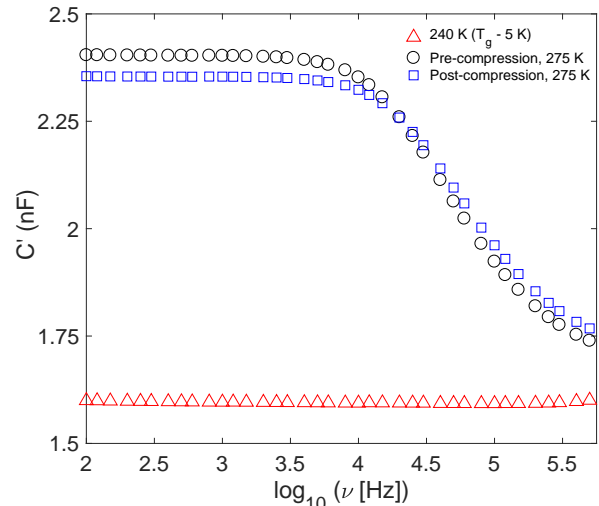


FIG. 3. Real part of the capacitance of 5PPE as a function of frequency at atmospheric pressure. Spectra at 275 K, before (black circles) and after (blue squares) compression at 100 MPa, show the alpha relaxation. Spectrum at 240 K (red triangles) corresponds to the glassy state, conditions at which the capacitance at high frequencies is dominated by atomic polarization. Data collected with the home-built capacitor presented in Fig. 2(d)

by rotational and atomic polarization respectively. In order to evaluate the phenomenon of pressure densification, similar spectra to that shown in Fig. 3 for 240 K ($T_g - 5$ K) were analyzed. At 275 K, the signal is dominated by the alpha relaxation of 5PPE and Fig. 3 displays two curves at this temperature, taken before and after compression to 100 MPa. Given the fact that both data at 275 K look similar, it seems plausible that the geometry of the home-built multilayer capacitor is nearly unmodified by compression to 100 MPa. To ensure that rotational polarization does not interfere with our data, the material density was inferred from the capacitance at 240 K and only the high-frequency flank of the spectra was taken into account.

The protocol used for the experiment is shown in Fig. 4. The state-point designated by the red circle (point B) was reached by the routes indicated by the solid and dashed black lines. In one case, the sample was cooled at atmospheric pressure, while in the second scenario the sample was first compressed at high temperatures, then cooled to the same temperature (point A), and finally decompressed to 0.1 MPa. We employed the same cooling rate in both cases. The same thermobaric protocol was applied on both capacitors.

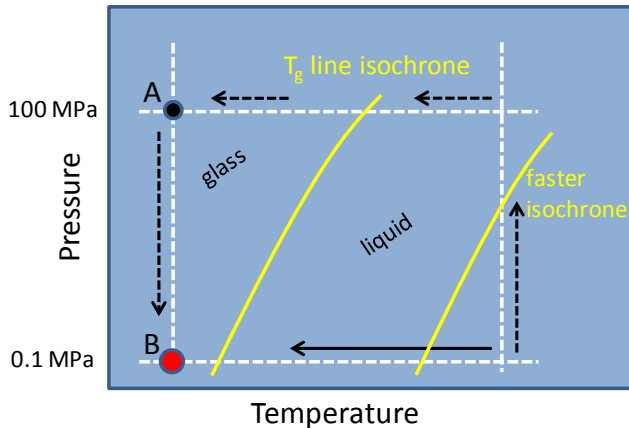


FIG. 4. Schematic description of the experimental protocol employed in this study. Two types of glasses were formed by following the solid (cooling at ambient pressure) and dashed (compression-cooling-decompression) black lines, which describe the two different routes for reaching the state point B. Glass and liquid domains are delimited by the T_g line isochrone. A faster isochrone at the high temperature flank is also indicated.

IV. RESULTS FROM THE TWO DIFFERENT CAPACITORS

Data from the air capacitor shown in Fig. 2(c) are presented in Fig. 5. We report the real part of the capacitance at a fixed frequency of 10 kHz for 5PPE glasses formed following the paths detailed in Fig. 4. Data are normalized to the capacitance of the 0.1 MPa glass and shown as a function of time. We studied decompression jumps from 100 and 60 MPa to ambient pressure. Black symbols correspond to a glass formed upon cooling at 0.1 MPa. When the glass is produced at the same cooling rate but starting from a liquid compressed at 100 (magenta) or 60 MPa (blue), the capacitance is significantly higher in comparison to the low-pressure glass, which is expected for a denser material [31, 37]. Then, pressure was released to 0.1 MPa, producing an immediate effect on the capacitive response as shown in Fig. 5. The capacitance suddenly decreases upon decompression and further decreases as a function of time. In the case of the pressure jump from 60 MPa, the capacitance immediately goes below the ambient pressure value, and this also happens after 8-30 hours in the case of the jumps from 100 MPa.

In Fig. 6 we show data from the home-built capacitor with Kapton® spacers. As stated above, the protocol used was the same as for the air capacitor. In this case, data are shown for 100-to-0.1 MPa jumps. It is seen that the capacitance of the post-compressed glass sample immediately goes below the normal glass value. It makes a fast undershoot and stays stable already after less than an hour.

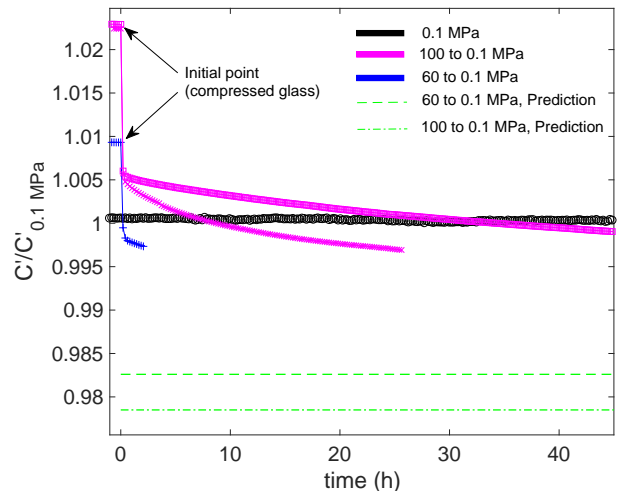


FIG. 5. Normalized capacitance at 10 kHz for glasses formed by cooling at 0.1 MPa (black circles) and glasses formed by cooling at high pressure and subsequent decompression to 0.1 MPa. Dielectric measurements collected with a multilayer air capacitor. Green lines correspond to the value expected according to the isomorph theory (absence of pressure densification in R-simple systems) for jumps from 60 and 100 to 0.1 MPa, together with our assumption that clamped glasses cannot flow radially (Eq. 7).

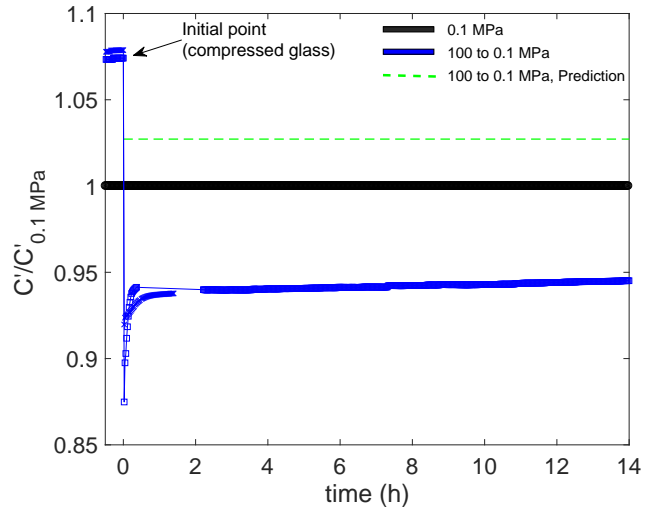


FIG. 6. Normalized capacitance at 10 kHz for glasses formed by cooling at 0.1 MPa (black) and glasses formed by cooling at 100 MPa and subsequent decompression to 0.1 MPa (blue). Dashed green line corresponds to the value expected according to the isomorph theory (absence of pressure densification in R-simple systems) for a jump from 100 to 0.1 MPa, together with our assumption that clamped glasses cannot flow radially (Eq. 7). These data were collected using the home-built capacitor described in Fig. 2(d).

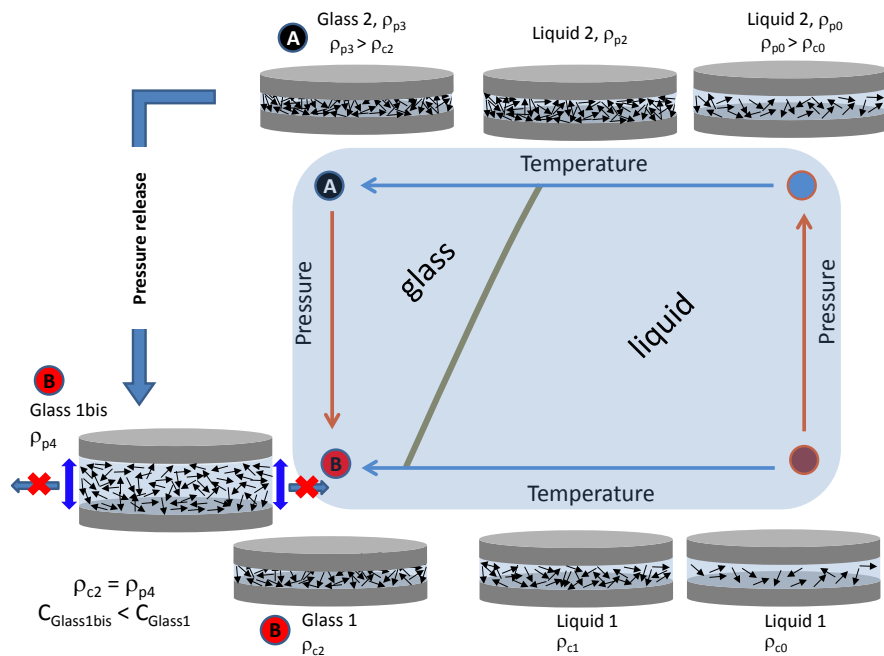


FIG. 7. Schematic description of two possible thermobaric routes for reaching the glassy state and the corresponding number density of dipoles (represented by black arrows) in a parallel-plate sample-filled capacitor. The restriction for the glass to flow tangentially after pressure release is indicated in the left bottom corner (Glass 1bis). The pressure release induces expansion in the vertical direction, moving the electrodes apart and consequently reducing the sample capacitance.

V. DISCUSSION

Studying the same sample using the same protocol but in two different capacitors clearly shows that the results depend not only on the properties of the glass but also on the sample capacitor. This emphasizes how important it is to understand the sample geometry when analyzing dielectric data in the aim of extracting density information. Another important result is that the capacitance measured after releasing pressure depends on time, particularly when using the air capacitor, which was also used in Ref. [16], where the authors unfortunately do not report how the pressure release affects the measured permittivity as a function of time.

If the glass formed at high pressure has higher ambient-pressure density than the glass formed at lower pressure, as is the case if the sample experiences pressure densification, the measured capacitance is higher in the densified sample. This would be the case due to the higher number density if the geometry is identical at the end of the two protocols, as assumed in Ref. [16]. Moreover, if the sample is compressed in the direction normal to the electrodes, the effect would be enhanced due to the shorter distance between the plates.

What we find in Fig. 5 and 6 is not a higher measured capacitance after the high pressure protocol, but in fact the opposite, a lower capacitance. This can be understood by the following argument. The glass at high pressure (point A) has a higher density than the glass at lower pressure (point B). With the higher density, most

scenarios also lead to more dipoles in absolute numbers between the electrodes of the capacitor than in the low pressure glass. It is for example obvious that high density leads to a larger number of dipoles in the case where it is assumed that the capacitor has the same geometry at high and low pressures. If there is no pressure densification, then the glass formed at high pressure will attain the density of the low pressure glass when the pressure is released. However, since it is a glass, it cannot flow, and it will be clamped in the tangential direction to the electrode plates. The only way to expand is normal to the electrodes and this will be done by pushing the electrodes apart (point B in Fig. 7, Glass 1bis). Consequently, the final result will be one where the glass formed at high pressure is in a capacitor with a larger distance between the electrodes and thus lower empty capacitance, while the actual density and dielectric constant of the two samples is the same. In the home-built capacitor, where there is no force keeping the electrodes together, this will happen abruptly, while it will happen to a lesser extent, and possibly over time, in the air capacitor where it requires bending of the electrodes. The slow response seen in the air capacitor could also be due to actual flow taking place. At 240 K, the alpha relaxation time for 5PPE is estimated to be 9.2×10^3 s and with a distance between the plates of 0.2 mm (air capacitor), this gives a characteristic flow-time of 2.3×10^7 s, following the argument in Ref. [11]. This flow time is long compared to the time scale of our experiment.

Considering the case of the home-built capacitor, we

can try to make a quantitative prediction of what a pure longitudinal expansion would give, starting from the value of the capacitance measured at high pressure. Assuming that the glass does not expand tangentially to the electrodes as the pressure drops, i.e., that it can only expand along the normal direction, the derivative of C_m with respect to pressure following Eq. (2) is given by

$$\frac{dC_m}{dp} = \varepsilon_\infty \frac{dC_g}{dp} + C_g \frac{d\varepsilon_\infty}{dp}. \quad (4)$$

Given that the longitudinal isothermal compressibility is defined as

$$\kappa_T = -\frac{1}{l} \left(\frac{\partial l}{\partial p} \right)_T, \quad (5)$$

where l corresponds to the distance between the electrodes (dimension in the direction of the flow), Eq. (4) can be written as [11]

$$\frac{1}{C_m} \frac{dC_m}{dp} = -\frac{\varepsilon_\infty + B(\varepsilon_\infty)}{\varepsilon_\infty} \kappa_T, \quad (6)$$

with $B(\varepsilon_\infty) = \frac{(\varepsilon_\infty - 1)(\varepsilon_\infty + 2)}{3}$.

At 0.1 MPa and 240 K, ε_∞ for 5PPE takes a value of 3.4 approximately. Thus, Eq. (6) can be reduced to

$$\frac{1}{C_m} \frac{dC_m}{dp} \simeq -\frac{2.3}{M}, \quad (7)$$

where M is the isothermal longitudinal modulus which is defined as the inverse of the longitudinal isothermal compressibility [38]. The longitudinal modulus is given by the bulk, K , and shear, G , moduli for isotropic solids through the equation $M = K + 4/3G$. From the longitudinal modulus M and, by means of Eq. (7), we can make a prediction of the measured capacitance for a 5PPE glass after releasing pressure. This is possible thanks to the availability of data for K and G for 5PPE at temperatures close to 240 K [39].

The decrease in capacitance calculated from this procedure for the home-built capacitor is shown as a green dashed line in Fig. 6. Curiously, the measured decrease in capacitance is much stronger, than what we get from this calculation. This could be due to cracking of the sample as a consequence of the abrupt change in pressure. This would lead to an even larger distance between the electrodes than a simple expansion. The resulting capacitance after decompression predicted by Eq. 7 is also shown in Fig. 5 for the air capacitor.

In Fig. 7 we show a schematic description of the situation explained above that allows one to understand why the post-compression glass presents a lower capacitance than the normal one. The number density of dipoles between the electrodes as a function of temperature and pressure is illustrated for the normal (Glass 1), compressed (Glass 2) and post-compression (Glass 1bis) glasses. The existence of isomorphs in strongly correlating liquids gives a theoretical foundation for arguing that, on cooling, both normal and compressed glasses of 5PPE explore state points in the phase diagram that remain *quasi-isomorphic* [21, 27]. Therefore, post-compression and normal glass should have similar densities that, together with the longitudinal expansion of the glass in the normal direction, would give rise to a lower value of the capacitance for the post-compression glass as indicated at the bottom of Fig. 7 (Glass 1bis, point B).

VI. CONCLUSIONS

Our data do not match the results reported by Casalini [16] on DC704 and do not indicate any significant pressure densification effects in 5PPE. While a signature of pressure densification would have given rise the capacitance to values higher than those shown by the 0.1 MPa glass, we observe here that the post-compression glasses present even lower values. In the case of the air capacitor we only see the lower values after significant waiting time. The discrepancy between the results could be explained if the data shown in Ref. [16] were measured immediately after the pressure was released.

We cannot determine on whether or not simple glass formers such as 5PPE can be pressure densified, but this investigation has highlighted the challenge of utilizing dielectric spectroscopy to tackle this problem effectively. The measured capacitance depends not only on the dielectric constant, but also on the geometry of the capacitor. In order to convert the measurements to density it is therefore crucial to understand the geometry. By comparing the results from two different capacitors with the same sample and protocol, we have demonstrated the importance of the geometry. Moreover, it should be stressed that a glass cannot be assumed to flow until waiting times are much longer than the alpha relaxation time. Density changes when releasing pressure in the glassy state therefore must take place by a solid-like type of deformation, which involves distortion of the dielectric cell.

ACKNOWLEDGMENTS

This work is supported by the VILLUM Foundation grant Matter (16515).

[1] K. Niss and T. Hecksher, The Journal of Chemical Physics **149**, 230901 (2018).

[2] M. D. Ediger, Annual Review of Physical Chemistry **51**,

- 99 (2000).
- [3] P. Debenedetti and F. Stillinger, *Nature* **410**, 259 (2001).
- [4] Q. Qin and G. B. McKenna, *Journal of Non-Crystalline Solids* **352**, 2977 (2006).
- [5] A. I. Nielsen, T. Christensen, B. Jakobsen, K. Niss, N. B. Olsen, R. Richert, and J. C. Dyre, *The Journal of Chemical Physics* **130**, 154508 (2009).
- [6] T. Hecksher, A. I. Nielsen, N. B. Olsen, and J. C. Dyre, *Nature Physics* **4**, 737 (2008).
- [7] M. Romanini, M. Barrio, R. Macovez, M. D. Ruiz-Martin, S. Capaccioli, and J. L. Tamarit, *Scientific Reports* **7**, 1346 (2017).
- [8] A. Grzybowski, K. Grzybowska, M. Paluch, A. Swiet, and K. Koperwas, *Phys. Rev. E* **83**, 041505 (2011).
- [9] H. W. Hansen, A. Sanz, K. Adrjanowicz, B. Frick, and K. Niss, *Nat. Commun.* **9**, 518 (2018).
- [10] C. Bauer, R. Böhmer, S. Moreno-Flores, R. Richert, H. Sillescu, and D. Neher, *Phys. Rev. E* **61**, 1755 (2000).
- [11] K. Niss, D. Gundermann, T. Christensen, and J. C. Dyre, *Phys. Rev. E* **85**, 041501 (2012).
- [12] K. Fukao and Y. Miyamoto, *Phys. Rev. E* **64**, 011803 (2001).
- [13] H. Yin, S. Napolitano, and A. Schönhals, *Macromolecules* **45**, 1652 (2012).
- [14] R. Inoue, T. Kanaya, T. Yamada, K. Shibata, and K. Fukao, *Phys. Rev. E* **97**, 012501 (2018).
- [15] K. Niss, *Phys. Rev. Lett.* **119**, 115703 (2017).
- [16] R. Casalini and C. Roland, *Journal of Non-Crystalline Solids* **475**, 25 (2017).
- [17] J. S. Tse, D. D. Klug, and Y. Le Page, *Phys. Rev. B* **46**, 5933 (1992).
- [18] R. G. Della Valle and E. Venuti, *Phys. Rev. B* **54**, 3809 (1996).
- [19] T. Rouxel, H. Ji, T. Hammouda, and A. Moréac, *Phys. Rev. Lett.* **100**, 225501 (2008).
- [20] A. Masuno, N. Nishiyama, F. Sato, N. Kitamura, T. Taniguchi, and H. Inoue, *RSC Advances* **6**, 19144 (2016).
- [21] D. Fragiadakis and C. M. Roland, *The Journal of Chemical Physics* **147**, 084508 (2017).
- [22] R. Casalini and C. M. Roland, *The Journal of Chemical Physics* **147**, 091104 (2017).
- [23] J. C. Dyre, *The Journal of Physical Chemistry B* **118**, 10007 (2014).
- [24] R. M. Kimmel and D. R. Uhlmann, *Journal of Applied Physics* **41**, 2917 (1970).
- [25] P. Destruel, B. Ai, and Hoang-The-Giam, *Journal of Applied Physics* **55**, 2726 (1984).
- [26] R. Casalini and C. Roland, *Phys. Rev. E* **69**, 062501 (2004).
- [27] N. Gnan, T. B. Schröder, U. R. Pedersen, N. P. Bailey, and J. C. Dyre, *The Journal of Chemical Physics* **131**, 234504 (2009).
- [28] I. V. Danilov, E. L. Gromnitskaya, and V. V. Brazhkin, *The Journal of Physical Chemistry B* **120**, 7593 (2016).
- [29] N. Gnan, C. Maggi, T. B. Schröder, and J. C. Dyre, *Phys. Rev. Lett.* **104**, 125902 (2010).
- [30] C. J. F. Böttcher, *Theory of electric polarization*, Vol. 1, 2 Edition, Elsevier Scientific Publishing Company (1973).
- [31] A. Schönhals and F. Kremer, *Broadband Dielectric Spectroscopy*, Springer-Verlag Berlin Heidelberg (2003).
- [32] L. A. Roed, D. Gundermann, J. C. Dyre, and K. Niss, *Journal of Chemical Physics* **139**, 01101 (2013).
- [33] L. A. Roed, K. Niss, and B. Jakobsen, *The Journal of Chemical Physics* **143**, 221101 (2015).
- [34] H. W. Hansen, B. Frick, S. Capaccioli, A. Sanz, and K. Niss, *The Journal of Chemical Physics* **149**, 214503 (2018).
- [35] B. Igarashi, T. Christensen, E. H. Larsen, N. B. Olsen, I. H. Pedersen, T. Rasmussen, and J. C. Dyre, *Review of Scientific Instruments* **79**, 045106 (2008).
- [36] W. Xiao, J. Tofteskov, T. V. Christensen, J. C. Dyre, and K. Niss, *Journal of Non-Crystalline Solids* **407**, 190 (2015).
- [37] M. Naoki and S. Koeda, *The Journal of Physical Chemistry* **93**, 948 (1989).
- [38] C. Kittel, *Introduction to Solid State Physics*, Seventh Edition, John Wiley & Sons, Inc. (1996).
- [39] T. Hecksher, *Relaxation in supercooled liquids: linear and nonlinear, mechanical and dielectric studies of molecular liquids*, Ph.D. thesis, IMFUFA, Roskilde University (2011).